

Biexciton crystal in a pentalayer $\text{MoSe}_2\text{-WSe}_2\text{-MoSe}_2\text{-WSe}_2\text{-MoSe}_2$

Yi Huang (黄奕)* and B.I. Shklovskii

School of Physics and Astronomy, University of Minnesota, Minneapolis, Minnesota 55455, USA

(Dated: July 26, 2022; Received July 26, 2022)

We study the gas of indirect dipolar excitons created by an interband illumination of pentalayer $\text{WSe}_2/\text{MoSe}_2/\text{WSe}_2/\text{MoSe}_2/\text{WSe}_2$. We show that two colinear indirect excitons bind into a linear biexciton with twice larger orthogonal to the pentalayer dipole moment. Two biexcitons with opposite dipolar directions attract each other at large distances and repel at short distances. Therefore, biexcitons form a crystal with an anti-ferroelectric square lattice. The electrostatic energy of this crystal per biexciton has a minimum at the biexciton concentration $n = n_c = 0.14d^{-2}$, where $d \sim 0.7$ nm is one layer thickness. At small illumination intensity when $n < n_c$ biexcitons condense into sparse droplets with $n = n_c$. Their luminescence is red shifted and independent on the light intensity.

Heterostructures of two-dimensional (2D) transition metal dichalcogenides (TMDC) demonstrated wide spectrum of correlated states of excitons. For example [1, 2], in bilayer $\text{MoSe}_2/\text{WSe}_2$, the type II band alignment of the MoSe_2 and WSe_2 monolayers allows the formation of spatially indirect excitons, in which an electron in MoSe_2 binds to a hole in WSe_2 and creates a dipolar exciton (see Fig.1). Parallel dipolar excitons repel each other at all distances between them or at different exciton concentrations tuned by the intensity of excitation by light. Because of the weak overlap of the electron and hole wave functions, these excitons decay slowly enough to form the correlated ground state, which minimizes their repulsion. It was observed [1, 2] that in $\text{MoSe}_2/\text{WSe}_2$ devices, the indirect exciton luminescence line is blue shifted due to the dipole-dipole repulsion of indirect excitons, and this effect becomes stronger as the light intensity increases.

It was predicted recently [3] that in a trilayer device [4, 5] $\text{WSe}_2/\text{MoSe}_2/\text{WSe}_2$ (WMW) and similar devices with identical hexagonal boron nitride (hBN) spacers between layers, repulsion of excitons at small distances is replaced by their attraction at larger distances. This happens because in a WMW device, the hole of an exciton is in either the upper or lower WSe_2 layer, while the electron is always in the middle layer. At large distances, two oppositely oriented dipolar excitons attract each other, while the repulsion takes over at short distances because electrons located in the middle layer approach each other. It was shown that the interaction energy of directed up and down dipolar excitons has a minimum near $n^{-1/2} = 2.8d$, where $d \sim 7$ nm [6] is the distance between two layers. The ground state of these excitons in a WMW device is a staggered square lattice of alternating up and down dipoles (see Fig. 3). The interaction energy per exciton of such a crystal has minimum at the concentration $n_c = 0.12d^{-2}$. Therefore, at low illumination intensities, when $n < n_c$, all excitons condense into droplets of the density n_c , which do not interact with each other.

Ref. [3] ignored the tunneling of an exciton hole between two possible locations in the lower and upper WSe_2 layer. For a single exciton this tunneling hybridizes two opposite orientations of a dipolar exciton and creates a quadrupolar dark exciton [6]. In a system of many interacting excitons this happens only at small enough concentration n when the energy

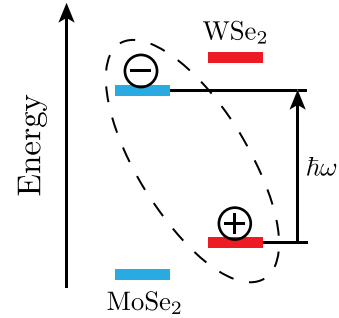


Figure 1. Band alignment in $\text{MoSe}_2/\text{WSe}_2$ bilayer. Absorption of a light quantum $\hbar\omega$ results in an electron in MoSe_2 layer and a hole in WSe_2 layer bound by the Coulomb interaction in an indirect exciton.

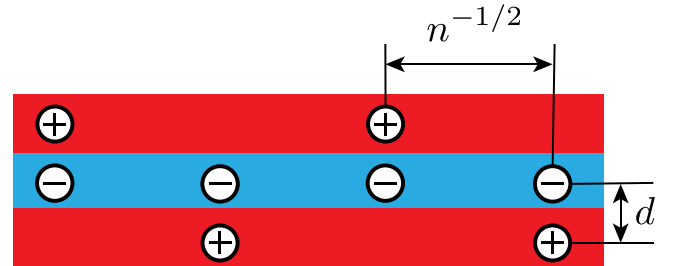


Figure 2. Schematic of a trilayer $\text{WSe}_2/\text{MoSe}_2/\text{WSe}_2$ for optical studies of spatially interacting indirect excitons. WSe_2 (first and third) layers are red and MoSe_2 (second) layer is blue. When the device is illuminated at low temperatures, the type II band alignment of neighboring $\text{WSe}_2/\text{MoSe}_2$ heterostructures allows the formation of indirect excitons consisting of an electron in MoSe_2 and a hole in WSe_2 . Excitons of opposite polarity attract each other and form a staggered crystal with alternating exciton dipoles.

splitting between symmetric and antisymmetric hole states is larger than the electrostatic energy required to invert the orientation of a dipolar exciton in the staggered crystal. According to Ref. [6] in WMW devices, the quadrupolar exciton phase should marginally lose to the staggered crystal at $n \sim n_c$.

A recent experimental paper [7] used optical methods to study exciton phases in a WMW device gated by transparent graphene layers on both sides separated by ~ 10 nm hBN spacers. The authors discovered the crystalline phase of indi-

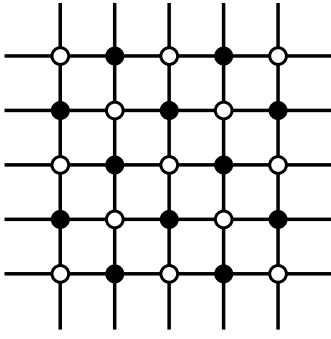


Figure 3. The top view of the anti-ferroelectric square lattice of alternating dipolar excitons or biexcitons. White (black) circles correspond to dipoles whose orientation points up (down). Straight lines are guides for eye.

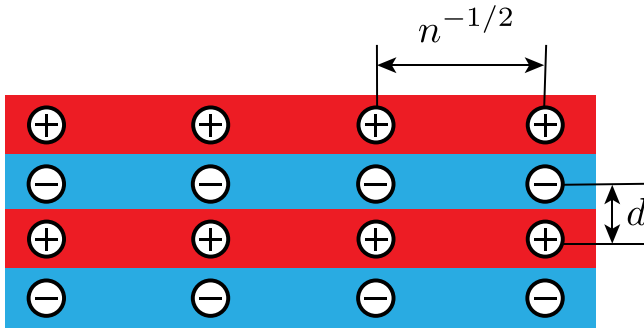


Figure 4. Tetralayer $\text{WSe}_2/\text{MoSe}_2/\text{WSe}_2/\text{MoSe}_2$ device. WSe_2 layers are red and MoSe_2 layers are blue. When the tetralayer device is illuminated at low temperatures, identical linear biexcitons are formed.

rect excitons. Indeed, they observed sharper peaks in photoluminescence due to stronger localization of excitons in moiré traps. They also measured directly the diffusion coefficient of excitons and showed that it decreases in the crystalline phase. The authors also attributed the low density dark exciton state to the predicted quadrupolar exciton [6], and showed how the transition from dark to bright exciton crystal happens by increasing the exciton concentration or by an applied electric field.

In this paper we extend our study of TMDC heterostructure to $\text{WSe}_2/\text{MoSe}_2/\text{WSe}_2/\text{MoSe}_2$ (WMWM) tetralayer and WMWMW pentalayer. In a WMWM tetralayer, all excitons pair and bind into identical linear dipolar biexcitons which repel each other and form a ferroelectric (see Fig. 4). On the other hand, in the pentalayer case, linear biexcitons can have two different dipole moment orientations (see Fig. 5). Two biexcitons with opposite directions of dipole moments attract each other at large distances. At small distances they strongly repel each other because they have charges of the same sign in three middle layers. This competition of attraction and repulsion leads to an anti-ferroelectric biexciton crystal in a WMWMW pentalayer. The side and the top view of this crystal are shown in Fig. 5 and Fig. 3.

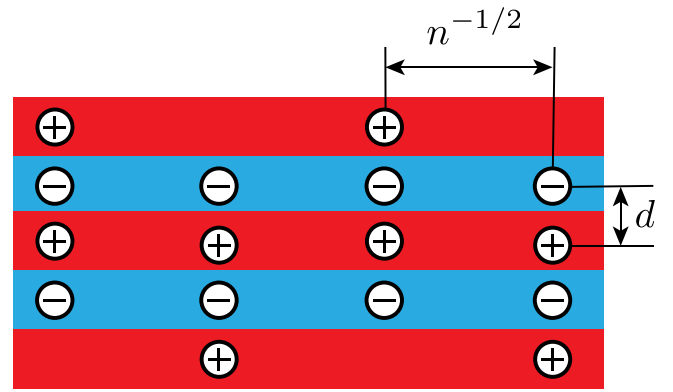


Figure 5. Pentlayer $\text{WSe}_2/\text{MoSe}_2/\text{WSe}_2/\text{MoSe}_2/\text{WSe}_2$ device. WSe_2 layers are red and MoSe_2 layers are blue. When the device is illuminated at low temperatures, linear biexcitons with alternating orientations are created. Biexcitons form a staggered square lattice, and the top view of which is shown in Fig. 3.

The electrostatic energy of the staggered crystal per biexciton in a pentalayer is calculated below. The result is shown by the full black curve as a function of nd^2 in Fig. 6, where n is the 2D concentration of biexcitons. This curve has a minimum at $n = n_c = 0.14d^{-2}$. In the same figure by the blue dash curve we reproduce the electrostatic energy per exciton of a staggered crystal in a WMW trilayer as a function of nd^2 , where n is the concentration of excitons [3]. We see that although both energies have minimum near close values of nd^2 , the cohesive energy of biexcitons is approximately 3 times larger. This allows to study the biexciton crystal in a WMWMW device at higher temperatures. (The reason for this larger attraction energy is that biexcitons in a pentalayer device have twice larger dipole moment than excitons in a trilayer device. Thus, the absolute value of the attraction energy is four times larger. Repulsion between two biexcitons at small distances is substantially larger than the case of excitons as well.)

Let us now show that the staggered crystal of biexcitons in a WMWMW device easily survives the competition of a crystal of quadrupolar dark biexcitons. Indeed, there is a possibility that the quantum mechanical tunneling of holes between bottom and top WSe_2 layers hybridizes two biexcitons with opposite orientations of their dipole moments into a symmetric quadrupolar dark biexciton. Whether the quadrupolar biexciton wins depends on the relationship between the quantum energy splitting of symmetric and antisymmetric biexciton states and the classical electrostatic energy cost of inverting the direction of a single biexciton in a fixed staggered lattice of its neighbors. We know that near $n = n_c$ in a WMW device, the staggered biexciton crystal phase has smaller energy and marginally dominates the phase diagram [6]. Now we should look at this competition in a pentalayer device.

Below we calculate the Coulomb energy cost ΔU of inverting the orientation of a dipolar biexciton in a WMWMW device, which can be done by applying an electric field in exper-

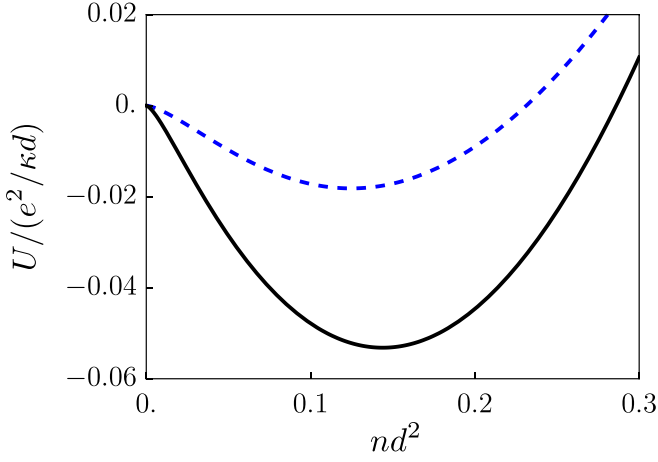


Figure 6. The full black curve shows the dimensionless electrostatic energy per biexciton $U/(e^2/\kappa d)$ in a staggered lattice (c.f. Fig. 3) versus the dimensionless biexciton density nd^2 in a WMWMW device. The blue dashed curve reproduces the electrostatic energy of a staggered lattice per exciton versus the dimensionless density of excitons nd^2 in a WMW device [3].

iments. It is plotted as a function of nd^2 in Fig. 7 together with the cost of inverting a dipolar exciton for a WMW device. (As in Fig. 6 for the full black curve n is understood as the concentration of biexcitons and for the blue dashed curve n represents the concentration of excitons.) We see that the former is approximately twice larger than the latter at $n \gtrsim n_c = 0.14d^{-2}$. On the other hand, quantum energy splitting in a WMWMW device is much smaller than in a WMW device. Indeed, the tunneling of a hole from the top WSe₂ layer to the bottom one requires simultaneous hopping of two holes. The hole from the middle WSe₂ layer hops to the bottom WSe₂ layer, while another hole of the same biexciton hops from the top WSe₂ layer to the middle WSe₂ layer. As a result in a WMWMW device, quantum energy splitting loses the competition by large margin and our classical theory is applicable practically at all interesting concentrations. Together with larger interaction energy per biexciton, namely, more stable staggered lattice, this makes the physics of a WMWMW device much simpler than that of a WMW one.

In the rest of this paper we explain how we arrived at results shown in Fig. 6 and Fig. 7. Without loss of generality, we pick a reference biexciton with its dipole moment pointing up as the reference point, and calculate its interaction with all other charges in the lattice. For convenience we separate U into four terms $U = U_{h1} + U_{e1} + U_{h2} + U_{e2}$, where $h1$, $h2$ ($e1$, $e2$) label the first and second holes (electrons) counting from the top in the reference biexciton. In the calculation of the biexciton interaction energy we ignore the interaction between electrons and holes of the same biexciton which are responsible for its self-energy.

Since the orientation of biexcitons alternates between neighboring sites which forms two sublattices labeled by \bullet (up) and \circ (down) in Fig. 3, the electrostatic energy consists of summa-

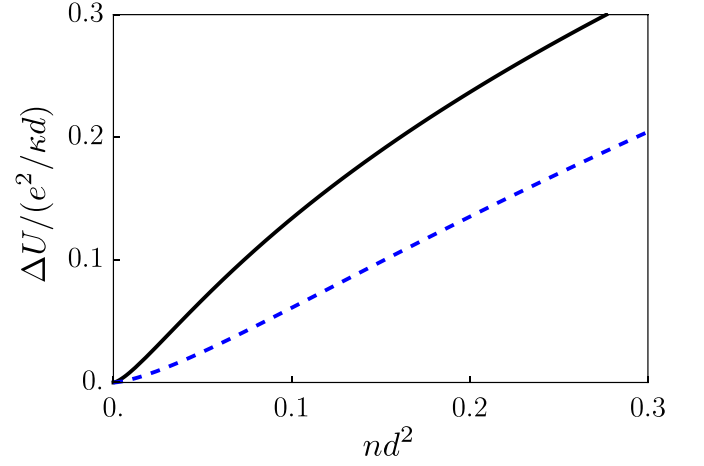


Figure 7. The full black curve shows the dimensionless energy cost $\Delta U/(e^2/\kappa d)$ of inverting the orientation of a biexciton in a penta-layer device (c.f. Fig. 5) by moving a hole from the top WSe₂ layer to the bottom WSe₂ layer versus the dimensionless biexciton density nd^2 . The blue dashed curve shows the energy of inverting an exciton in a trilayer device (c.f. Fig. 2) by moving a hole from the top WSe₂ layer to the bottom one versus the exciton density nd^2 .

tion over two sublattices (r_α is the 2D coordinate of a biexciton α) as follows:

$$U_{h1} = \frac{e^2}{2\kappa} \sum_{\alpha \neq 0}^{\circ} \left(\frac{1}{\sqrt{r_\alpha^2 + (2d)^2}} + \frac{1}{\sqrt{r_\alpha^2 + (4d)^2}} - \frac{1}{\sqrt{r_\alpha^2 + d^2}} - \frac{1}{\sqrt{r_\alpha^2 + (3d)^2}} \right) + \frac{e^2}{2\kappa} \sum_{\alpha \neq 0}^{\bullet} \left(\frac{1}{\sqrt{r_\alpha^2}} + \frac{1}{\sqrt{r_\alpha^2 + (2d)^2}} - \frac{1}{\sqrt{r_\alpha^2 + d^2}} - \frac{1}{\sqrt{r_\alpha^2 + (3d)^2}} \right), \quad (1)$$

$$U_{e1} = \frac{e^2}{2\kappa} \sum_{\alpha \neq 0}^{\circ} \left(\frac{1}{\sqrt{r_\alpha^2}} + \frac{1}{\sqrt{r_\alpha^2 + (2d)^2}} - \frac{1}{\sqrt{r_\alpha^2 + d^2}} - \frac{1}{\sqrt{r_\alpha^2 + (3d)^2}} \right) + \frac{e^2}{2\kappa} \sum_{\alpha \neq 0}^{\bullet} \left(\frac{1}{\sqrt{r_\alpha^2}} + \frac{1}{\sqrt{r_\alpha^2 + (2d)^2}} - \frac{2}{\sqrt{r_\alpha^2 + d^2}} \right), \quad (2)$$

$$U_{h2} = \frac{e^2}{2\kappa} \sum_{\alpha \neq 0}^{\circ} \left(\frac{1}{\sqrt{r_\alpha^2}} + \frac{1}{\sqrt{r_\alpha^2 + (2d)^2}} - \frac{2}{\sqrt{r_\alpha^2 + d^2}} \right), \quad (3)$$

$$\begin{aligned}
U_{e2} = & \frac{e^2}{2\kappa} \sum_{\alpha \neq 0}^{\circ} \left(\frac{1}{\sqrt{r_\alpha^2}} + \frac{1}{\sqrt{r_\alpha^2 + (2d)^2}} - \frac{2}{\sqrt{r_\alpha^2 + d^2}} \right) \\
& + \frac{e^2}{2\kappa} \sum_{\alpha \neq 0}^{\bullet} \left(\frac{1}{\sqrt{r_\alpha^2}} + \frac{1}{\sqrt{r_\alpha^2 + (2d)^2}} \right. \\
& \left. - \frac{1}{\sqrt{r_\alpha^2 + d^2}} - \frac{1}{\sqrt{r_\alpha^2 + (3d)^2}} \right), \quad (4)
\end{aligned}$$

where κ is the dielectric constant of the system and $\alpha \neq 0$ means we exclude the coordinate origin in the summation. As a result, we obtain the interaction energy $U = U_{h1} + U_{e1} + U_{h2} + U_{e2}$:

$$U = \frac{e^2}{2\kappa d} f(nd^2), \quad (5)$$

where the dimensionless function $f(x)$ is given by

$$\begin{aligned}
f(x) = & 2\sqrt{x} \sum_{i=1}^{\infty} \sum_{j=0}^{\infty} \left(\frac{4}{\sqrt{i^2 + j^2}} + \frac{4}{\sqrt{i^2 + j^2 + 2^2x}} - \frac{6}{\sqrt{i^2 + j^2 + x}} - \frac{2}{\sqrt{i^2 + j^2 + 3^2x}} \right) \\
& + 2\sqrt{x} \sum_{i=0}^{\infty} \sum_{j=0}^{\infty} (2 - \delta_{j0}) \left(\frac{1}{\sqrt{(2i+1)^2 + (2j)^2 + 4^2x}} - \frac{1}{\sqrt{(2i+1)^2 + (2j)^2}} \right) \quad (6)
\end{aligned}$$

Next we calculate the Coulomb energy cost to flip the orientation of a biexciton in the staggered lattice of a WMWMW pentalayer (c.f. Fig. 5). By moving the hole $h1$ of a reference biexciton in the top WSe₂ layer to the bottom WSe₂ layer and relabel it as $h3$, we find its electrostatic energy as

$$\begin{aligned}
U_{h3} = & \frac{e^2}{2\kappa} \sum_{\alpha \neq 0}^{\circ} \left(\frac{1}{\sqrt{r_\alpha^2}} + \frac{1}{\sqrt{r_\alpha^2 + (2d)^2}} \right. \\
& \left. - \frac{1}{\sqrt{r_\alpha^2 + d^2}} - \frac{1}{\sqrt{r_\alpha^2 + (3d)^2}} \right) \\
& + \frac{e^2}{2\kappa} \sum_{\alpha \neq 0}^{\bullet} \left(\frac{1}{\sqrt{r_\alpha^2 + (2d)^2}} + \frac{1}{\sqrt{r_\alpha^2 + (4d)^2}} \right. \\
& \left. - \frac{1}{\sqrt{r_\alpha^2 + d^2}} - \frac{1}{\sqrt{r_\alpha^2 + (3d)^2}} \right). \quad (7)
\end{aligned}$$

The energy cost of inverting a biexciton orientation is then given by $\Delta U = U_{h3} - U_{h1}$. This energy is plotted as the full black curve in Fig. 7, where the energy cost to flip an exciton for a WMW trilayer is shown by the dashed blue curve for comparison. At very small concentration $nd^2 \rightarrow 0$, we have $\Delta U \propto n^{3/2}$ with the coefficient of a pentalayer device 4 times larger than that for a trilayer. At larger concentration $n \gtrsim n_c = 0.14d^{-2}$, the energy cost to flip a biexciton in a pentalayer is 2 times larger than to flip an exciton in a trilayer.

Our theory assumes the electrons (holes) are point-like particles located in the middle of a layer. This is a good assumption if $n^{-1/2} \gg a$, where a is the localization length of electrons (holes). Using an estimate $a = \hbar/\sqrt{2m^*E_b}$, where the effective mass $m^* \sim 0.5m_0$ [8], m_0 is the free electron mass, and $E_b \sim 250$ meV [9, 10] is the binding energy of an exciton, we get $a \sim 0.6$ nm. On the other hand, $n_c^{-1/2} \sim 2.7d \sim 1.9$ nm, so our classical theory is correct for $n \lesssim n_c$ and needs a correction for larger n where substantial overlap of wave func-

tions leads to biexcitons decay to free excitons and eventually to electron-hole plasmas. This, however, does not change our prediction that at $n < n_c$ biexcitons condense into droplets with $n = n_c$, which produce red shifted photoluminescence independent on the light intensity.

Above we dealt with contactless WMWMW heterolayer designed for optical studies. It can be augmented by a common contact, which allows to gate the heterolayer by the top and bottom gates [7]. One can imagine a more challenging device in which two MoSe₂ and three WSe₂ layers are contacted separately allowing to study the non-trivial M-W capacitance between them. Theory of such a M-W capacitance was the main subject of previous study of a WMW device [3]. In a WMWMW device, M-W capacitance behaves similarly to the capacitance of WMW layer [3]. It can be calculated using the energy of the biexciton crystal of a pentalayer $U(n)$ shown in Fig. 6, but this calculation goes beyond the scope of this paper.

We are grateful to M. Sammon for helpful discussion. Y.H. gratefully acknowledges support from Larkin Fellowship at the University of Minnesota.

* Corresponding author: huan1756@umn.edu

- [1] P. Rivera, J. R. Schaibley, A. M. Jones, J. S. Ross, S. Wu, G. Aivazian, P. Klement, K. Seyler, G. Clark, N. J. Ghimire, J. Yan, D. G. Mandrus, and X. Xu, *Nat. Comm.* **6**, 6242 (2015).
- [2] E. V. Calman, L. H. Fowler-Gerace, L. V. Butov, D. E. Nikonov, I. A. Young, S. Hu, A. Mischenko, and A. K. Geim, arXiv e-prints, arXiv:1901.08664 (2019), [arXiv:1901.08664](https://arxiv.org/abs/1901.08664) [cond-mat.mes-hall].
- [3] M. Sammon and B. I. Shklovskii, *Phys. Rev. B* **99**, 165403 (2019).
- [4] M. Baranowski, A. Surrente, L. Kłopotowski, J. M. Urban, N. Zhang, D. K. Maude, K. Wiwatowski, S. Mackowski, Y.-C. Kung, D. Dumcenco, A. Kis, and P. Plochocka, *Nano letters*

- 17, 6360 (2017).
- [5] C. Choi, J. Huang, H.-C. Cheng, H. Kim, A. K. Vinod, S.-H. Bae, V. O. Özçelik, R. Grassi, J. Chae, S.-W. Huang, X. Duan, K. Kaasbjerg, T. Low, and C. W. Wong, *npj 2D Materials and Applications* **2**, 30 (2018).
- [6] Y. Slobodkin, Y. Mazuz-Harpaz, S. Refaely-Abramson, S. Gazit, H. Steinberg, and R. Rapaport, *Phys. Rev. Lett.* **125**, 255301 (2020).
- [7] Y. Bai, S. Liu, Y. Guo, J. Pack, J. Wang, C. R. Dean, J. Hone, and X. Y. Zhu, “Evidence for exciton crystals in a 2d semiconductor heterotrilaier,” (2022), [arXiv:2207.09601](https://arxiv.org/abs/2207.09601) [cond-mat.mes-hall].
- [8] For electrons in MoSe₂ the effective mass is $m_e^* = 0.49 m_0$ [11, 12] and for holes in WSe₂ is $m_h^* = 0.42 m_0$ [13].
- [9] R. Gillen and J. Maultzsch, *Phys. Rev. B* **97**, 165306 (2018).
- [10] H. C. Kamban and T. G. Pedersen, *Scientific Reports* **10**, 5537 (2020).
- [11] E. Liu, J. van Baren, C.-T. Liang, T. Taniguchi, K. Watanabe, N. M. Gabor, Y.-C. Chang, and C. H. Lui, *Phys. Rev. Lett.* **124**, 196802 (2020).
- [12] E. Liu, E. Barré, J. van Baren, M. Wilson, T. Taniguchi, K. Watanabe, Y.-T. Cui, N. M. Gabor, T. F. Heinz, Y.-C. Chang, and C. H. Lui, *Nature* **594**, 46 (2021).
- [13] P. V. Nguyen, N. C. Teutsch, N. P. Wilson, J. Kahn, X. Xia, A. J. Graham, V. Kandyba, A. Giampietri, A. Barinov, G. C. Constantinescu, N. Yeung, N. D. M. Hine, X. Xu, D. H. Cobden, and N. R. Wilson, *Nature* **572**, 220 (2019).